# A Topology Inference Method of Cortical Neuron Networks based on Network Tomography and the Internet of Bio-Nano Things

Michael Taynnan Barros, Harun Siljak, Alaa Ekky and Nicola Marchetti

***Abstract*—This letter presents a topology inference technique for neuronal networks of the cortex of the human brain based on network tomography theory. We envision that this technique will be used for high-resolution and high-precision brain tissue tomography and imaging using principles of the Internet of Bio-Nano Things. Our network tomography solution relies on the classification of processed data of spike delay and synaptic weight functions of neuronal network activity. For a 6-layer cortical neural network, we achieved 99.27% of accuracy using the Decision Tree machine learning technique for individual neurons, 2-leaf and 4-leaf star topologies of neuronal networks.**

***Index Terms*—IoBNT, Molecular Communications, Network Tomography, Topology Inference, Machine Learning**

## I. Introduction

The tomography of the brain has historically provided medical practitioners with an advanced technological apparatus for observing and diagnosing the tissue state and its possible pathologies. More recently, image processing techniques from computerised tomography became an essential part of the diagnosis of brain disorders. However, current computerised tomography is still far from achieving high-resolution characterisation of brain activity with network-level precision. The most advanced computerised brain tomography, within the minimally invasive space, is based on photoacoustics can only reach precision at functional brain regions [1]. The efficiency of diagnosis of brain disorders can be improved with techniques that precisely map neuron connections at the tissue level, as well as allow in-vivo characterisation of their activity, based on advanced minimally invasive technologies.

The monitoring of in-vivo cellular activity will potentially be achieved with implantable bio-nano devices for future theranostics technology [2]. The idea behind this technology is that cellular signals can be measured at the intracellular level, intercellular level and/or extracellular level with biocompatible bio-nano devices that interface with organs using connections to individual cells. The newly proposed Internet of Bionano Things (IoBNT) [3], envisions that these devices can have added programmable functionalities and be remotely controlled by developing technologies that allow their integration with the Internet. The above-mentioned principles inspire researchers to design minimally invasive solutions based on bio-nano sensing that can assist in the future technologies for the brain, and in our case, we want to develop an IoBNT approach for the next-generation tomography of brain tissues.

M. T. Barros is with the TSSG/Waterford Institute of Technology, Ireland, and CBIG at BioMediTech Unit, Faculty of Medicine and Health Technology of the Tampere University, Finland. H. Siljak, A. Ekky and N. Marchetti are with Trinity College Dublin, Ireland. The main contact is: mbarros@tssg.org

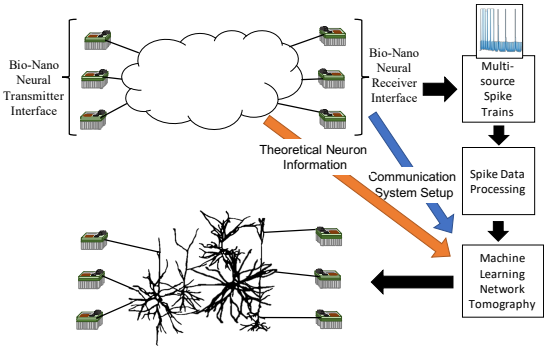


Fig. 1: The envisioned network tomography system.

In IoBNT, bio-nano devices transmit information using tissue as a communication channel through the molecular communications paradigm [4], [5]. We envision that this system will be used to create a distributed sensor system that characterises the whole tissue using a limited number of bio-nano sensors. This opens the possibility to create a technology that sends back-back signals between bio-nano devices that can be measured in different points of the tissue to infer the actual network topology of cells. Such an approach is called network tomography in computer networks [6], and is depicted for our scenario in Fig. 1. Since the biological neuron networks exhibit a great difference of transmission and signal propagation depending on the type of cells [7], inferring the organisation of these cells based on network topology models is very challenging but also promises to achieve a precise inference of the tissue state, or of the channel state.

To this end, we propose the usage of network tomography for topology inference of neuronal cells in the brain towards high-resolution characterisation of neuronal activity, or brain neuron network mapping. We use the approach proposed by Tsang *et. al.* that relies on estimation based on a delay measure for topology inference [8] and extend it to include synaptic weight, which is a natural neuronal molecular communication process [9]. We use machine learning as our classification method for different types of neuronal networks. We use the NEURON simulator with models from the Blue Brain Project to create a realistic representation of cortical microcircuit networks. Then we apply a Decision Tree model for the inference of three types of topologies, i.e., individual neurons, 2-leaf star and 4-leaf star. Our results show that 99.34% of

accuracy can be achieved with a delay of 5ms and synaptic weight of 1.5, which are promising results that pave the way for more research on this technology aiming to reliably infer larger topologies structures and their eventual complex communication patterns in the near future.

## II. Network Tomography for Molecular Communication Nanonetworks

Inspired from the multi-compartment model of the Neocortical Microcircuit Collaboration Portal (NMC), here we present the signal propagation model of a cortical neuron network that is directly implemented in the NEURON simulator as well as the network tomography theory with delay and synaptic weight measures. In Cable theory, each neuron type can be simplified to a sequence of capacitances and resistances in parallel and then grouped to form an entire cortical microcircuit. The *Telegrapher's Equation* and the *Compartment Models* yields to the following famous equation [10]

$$\tau \frac{\partial V}{\partial t} - \lambda^2 \frac{\partial^2 V(x)}{\partial x^2} = V_L - V, \tag{1}$$

in which $\tau$ is the leakage conductance decay rate, $V$ is the membrane voltage, $x$ is the neurite[1] axis length, $\lambda$ is the spatial coordinate decay rate and $V_L$ is the leakage (or resting) potential of the cell. If we assume two neurons, labelled $\eta$ and $\omega$, the direction communication from $\omega$ to $\eta$ with conductance $g_{\eta\omega}$, can be incorporated into Eq. (1) as suggested by the *Rall* Model [11], and represented as follows:

$$\begin{aligned} &\tau \frac{\partial V_\eta}{\partial t} - \lambda^2 \frac{\partial^2 V_\eta}{\partial x^2} = \\ &V_L - V_\eta + \delta(x - x_g) g_{\eta\omega}(V_\omega - V_\eta) + \sum_n I_{ion_{\eta,\omega,n}} \end{aligned} \tag{2}$$

in which $\delta(.)$ is the Dirac delta function, $x_g$ is the compartment location, and $I_{ion}$ is the current from the $n$-th channel for chemical synapses. The ionic channels depend on the specific neuron chemical synapses in each cortical layer. Here they are simplified to fit experimental data. We use the NEURON simulator that discretises both space and time, thus replacing the partial differential equation by a coupled system of ordinary differential equations (ODEs). This is called compartmental modelling and has been introduced to neural modelling by [11]. The spatial discretisation yields to a Kirchhoff's current law type equation described as:

$$c_{x_g} \frac{\mathrm{d}V_{x_g}}{\mathrm{d}t} + \sum_n I_{ion_{x_g,n}} = \sum_k \frac{V_k - V_{x_g}}{R_{x_g,k}} \tag{3}$$

in which $c_{x_g}$ is the membrane capacitance of the compartment, and $R$ the resistance. The right-hand side of Eq. (3) is the sum of axial currents that enter this compartment from its adjacent neighbours, including neighbouring cells in case of cellular border compartments. When $V_{x_g} > th$, where $th$ is the excitation threshold, the neuron will produce a spike. Over time, it will produce a set of spikes leading to a signal $S(t)$, which represents the spike train.

[1]projection from the cell body of a neuron, which can be either an axon or a dendrite.

Typical network tomography can be reduced to a linear model of a vector of measurements $\mathbf{y}$, which represents a set of all the calculated multi-domain measurements of the network that is defined as $\mathbf{y} = \mathbf{A}(\theta_\mathbf{d} \circ \theta_\mathbf{w}) + \epsilon$, in which $\mathbf{A}$ is a connection probability matrix between cortical neurons, $\theta_\mathbf{d}$ is a vector of signal propagation delay, $\theta_\mathbf{w}$ is a vector of signal propagation synaptic weight, $\epsilon$ is a generic noise matrix with same shape as $\mathbf{A}$ and $\circ$ is the Hadamard product. Since we consider small topologies, we can assume that all elements in $\epsilon$ are 0. Now we use the following equations for calculating all the delay measures for $\theta_d$ and the synaptic weight measures for $\theta_w$. Let us define $d_k = d_t - d_{t-1}, \{d_t, d_{t-1}\} \in S(t)$, in which $d_t$ is the time of the current spike, $d_{t-1}$ is the time of the previous spike, and the average delay will be $D = (1/K)(\sum_{k=0}^{K} d_k)$, where $K$ is the total amount of delay measures. The synaptic weight values $W$ in $\theta_\mathbf{w}$ are considered to be constant in the NEURON models. In this letter, we aim to demonstrate the impact of machine learning-based inference of network tomography as an advancement of the work by Tsang *et. al.* [8], and therefore the communication system between bio-nano machines is considered ideal and the study of its scalability is left for future work. In the next sections, we will build a Decision Tree Classification model based on the values of $\mathbf{y}$ for different topologies.

## III. Performance analysis

We aim to evaluate the impact of the vector of measurements $\mathbf{y}$, in particular variations of spike delay and synaptic weight, on the prediction of an individual neuron, a 2-leaf star and 4-leaf star topologies. We use metrics such as accuracy, precision and recall to measure the effectiveness of the proposed inference technique. We define accuracy as the percentage of correctly classified topologies, precision represents the percentage of topologies that are properly linked to the predicted class, and recall represents the percentage of topologies that are correctly identified.

*1) Simulation Setup:* The cerebral cortex or neocortex consists of six layers where the majority of neurons are arranged vertically while the most abundant neurons are the efferent pyramidal cells. We used experimental data to adjust Eq. (3) of these cell types from the digital reconstruction of the microcircuitry of somatosensory cortex[2]. Our models comprised of six neurons, one from each layer with different morphology types (m-types). For simplicity neurons were arbitrarily picked, but the m-type was dependent on whether the pathways were excitatory or inhibitory. This was important for the spike train analysis as excitatory neurons generate a net positive voltage that exceeds the threshold potential and causes an Action Potential. Thus, the neuron with excitatory properties was the one stimulated. One neuron from each layer was used in three topologies. The individual cell used was from Layer 5. The two-leaf topology consisted of neurons from Layers 1, 4 and 6 while the four-leaf topology consists of neurons from Layers 1, 2/3, 4, 5 and 6 respectively. Morphological and biophysical details of the neurons were initialized before arranging them

[2]The experimental data of juvenile rat, the digital reconstruction and the simulation results are available at the Neocortical Microcircuit Collaboration Portal (NMC Portal; https://bbp.epfl.ch/nmc-portal)

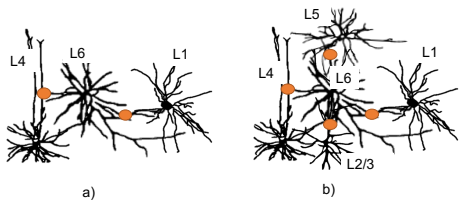


Fig. 2: The used topologies (a) Two Leaf Star (b) Four-Leaf Star

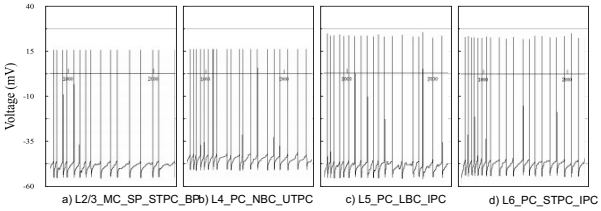


Fig. 3: Spike Trains for Individual Neuron Model of L5_DBC_cAC

in a star topology on a unit circle for Eq. (3). The base of the star was placed at the origin so L6 was placed at (0, 0, 0) three dimensional Cartesian coordinates for both topologies. This was enough for the individual neuron model. The two-leaf topology is displayed in Fig. 2 (a), and is defined with L1 placed to the right of L6 using the unit circle with co-ordinates ($2\pi$, 0, 0). L4 was placed to the left of the origin with co-ordinates ($-\pi$, 0, 0). For the four-leaf topology, Fig. 2 (b), the two-leaf topologies configuration is used by two other cells, and L2/3 and L5 models were added. L2/3 model was placed below L6 with co-ordinates (0, $3\pi/2$, 0) while L5 was placed above L6 with co-ordinates (0, $\pi/2$, 0). The neuron at the origin was stimulated in multiple points using virtual synapses which will drive the cell through synaptic events (located in orange in Fig. 2). This is important to generate data for training the machine learning algorithm used for the inference process. An axon from the cell at L6 is connected to a synapse in the middle of the dendrite on the target cell with a certain connection probability. The neuron models were connected and stimulated with a simulation time of 1000ms. From the spike train signals we obtained the voltage, time, delay and frequency of spikes, number of spikes and average power spectral density of each spike were recorded and considered as machine learning features. To access the neuron experimental data in the NMC portal, the NEURON simulator was used and RapidMiner, a machine learning tool, was used for inferring cortical topologies. We used NEURON to generate $\mathbf{y}$ values creating an overall system data set. Then we created a Decision Tree Classification model implemented in RapidMiner with a 30-70 split (30% testing and 70% training) to classify the topologies investigated running a cross-validation methodology. We chose Decision Trees-based models due to low computing complexity in both training and testing phases, which is more suitable to be implemented in bio-nano devices. However, the performance of these models might change, and should be investigated in future works.

*2) Classification of Individual Neuron Models:* A Layer 5 model was investigated for the individual neuron analysis, specifically the L5_DBC_cAC model. A combination of 4 presynaptic m-types originating from layers L2/3 (MC_SP_STPC_BP), L4 (PC_NBC_UTPC), L5 (PC_LBC_IPC) and L6 ( PC_STPC_IPC) respectively. The spike trains for each simulation are shown, see Fig. 3. The spike train in Fig. 3 tend to follow the same pattern at the start of the simulation where the neuron cell remains at a stable voltage. However, they deviate at the occurrence of the first spike. The first spike occurs at 783ms in Fig. 3 (a), but that is not the case for Fig. 3 (d) where it occurs at 765ms. Another significant difference is the number of spikes present in the spike train; Fig. 3 (d) contains 100 spikes while Fig. 3 (a) contains 71 spikes. A very interesting observation was that a presynaptic m-type from a Pyramidal Cell (PC) had a greater number of spikes than a presynaptic m-type from a Martinotti Cell (MC) during this simulation. This shows that when different m-types experience the same stimulation, they react in different ways. Moreover, PC type neurons (Fig. 3 b,c and d) observed a smaller delay between spikes as well as more frequent spikes when compared to MC neuron (Fig. 3 a). This validates our model based on the findings in [12] where the pyramidal cell in Layer 2/3 experienced higher frequency spikes when compared with other m-types in higher layers. We analysed the performance of classifying individual neuron models. The obtained accuracy results in predicting the presynaptic m-types was 96.95%. Obtaining a high accuracy result paves the way for investigating multiple neuron models connected in a star topology.

*3) Inferring Multiple Neuron Models in a Network:* Here we aim to focus our analysis on three different topologies that were previously presented: Individual Neuron, 2-Leaf Star and 4-Leaf Star. We attempt to investigate the effect of the synaptic weight (herein called weight) and delay only on the 2-Leaf and 4-Leaf topologies inference-based classification. We directly obtain the inference results from the classification outputs for analysis simplicity, however probabilistic approaches can be used to increase the accuracy of inference results, for example, using *Maximum Likelihood* methods. Fig. 4 a), b) and c) show the results for the comparison of spike trains with weights (W) 1.5 and 3 combined with delays (D) 5ms and 10ms for the 2-Leaf (top) and 4-Leaf topologies (bottom). For $W = 1.5$ and $D = 5$ms 4 (see Fig. 4a), the cell located at the base of the star in both topologies was stimulated for 1000ms and the time and voltage were recorded. From 0 to 100ms, the cell experiences multiple synaptic events with a delay of 5ms. The 4 star-leaf topology exhibits a continuous spike train response compared with the 2-leaf topology. This behaviour results from the composition (e-type) present in the cell, named continuous Adapting (cAD), where the cell continuously adapts to changes or synaptic events. For $W = 1.5$ and $D = 10$ms (see Fig. 4b), the delay between synaptic events has increased resulting in a decrease in the number of spikes over the simulation run time. This delay change is independent of the topology thus affecting all neurons. For $W = 3$ and $D = 5$ms (see Fig. 4c), unlike doubling the delay, the result of doubling the weight increases the number of spikes for the same simulation run time. The voltage is not affected as increasing weight only increases the number of spikes and frequency of spikes. We designed a decision tree model using the RapidMiner tool to determine topologies given a training phase with the

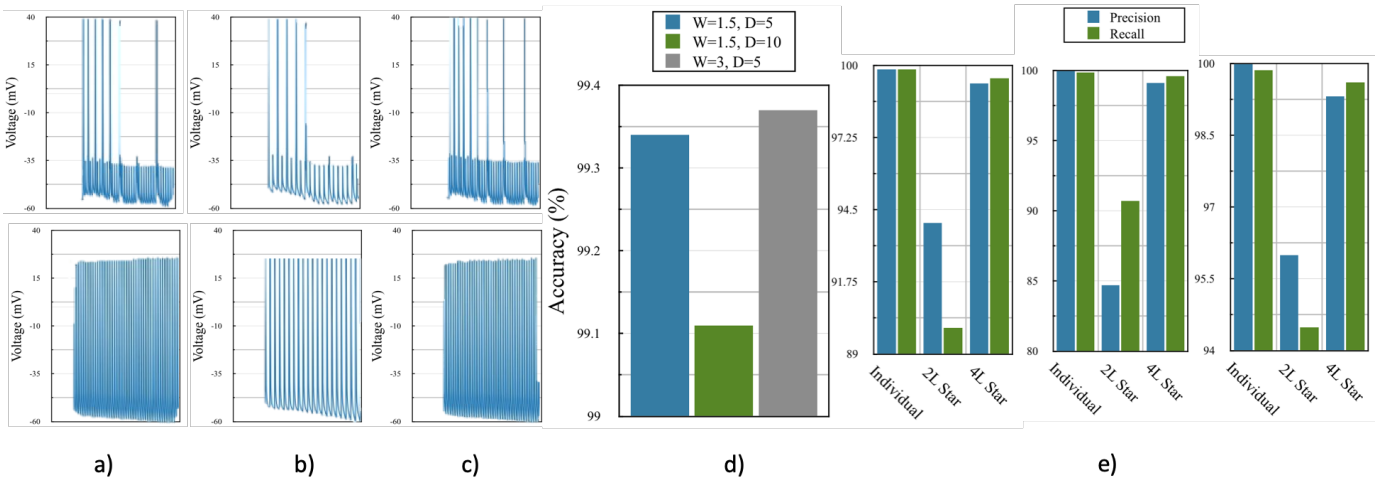


Fig. 4: Results from the topology inference technique a decision tree classification algorithm. a) show spike train for a 2-Leaf (top) and a 4-Leaf (bottom) star topology with weight of 1.5 and delay of 5ms b) same scenario now with the weight 1.5 and delay 10ms c) same scenario now with the weight 3 and delay 5ms d) accuracy results for all weights (W) and delays (D) e) precision and recall results for the individual, 2-Leaf and 4-Leaf star topologies for W=1.5 and D=5ms (left), W=1.5 and D=10ms (center) and W=3 and D=10ms (left).

neuronal communication parameters as features, including the delay, synaptic weight, and spike rate. Overall accuracy of the classification was obtained for all analysed delay and weight values (see Fig. 4d). An overall accuracy of 99.27% was obtained for the classifier on the entire data set, with all the weights and delay values for all topologies. Varying delay and weight both affect the overall accuracy when classifying topologies. Doubling the delay gives the lowest overall accuracy at 99.11% as the number of spikes and time are not enough for predicting topologies. However, doubling the weight gives a higher accuracy at 99.37%. This accuracy was obtained for small star topologies which contained a maximum of 5 neuron models. Class precision and class recall were used to evaluate the quality of prediction for each application class (see Fig. 4e). The lowest value of class precision was obtained when predicting the 2 Leaf topology as 63 of the 67 instances were correctly classified but the remaining 4 were misclassified as the 4 Leaf topology. Similarly, the class recall was lowest for the 2 Leaf topology. An increase in misclassification leads to a decrease in class recall for that same topology. It is evident that spikes might occur at the same times in both 2 Leaf and 4 Leaf topologies with the delay increase, leading, thereafter, to a decrease in overall accuracy and recall.

## IV. Conclusion

In this letter, we propose a network tomography technique based on delay and synaptic weight analysis to infer cortical circuits of the brain towards the next-generation of computerised imaging based on bio-nano sensing technology. We analysed the performance of our approach based on the Decision Tree technique. We obtained an overall accuracy of 99.27% including all dataset for varying spike transmission delay and synaptic weight. In reality, the cortical circuit contains hundreds of thousands of connected neuron models which is very challenging to infer with the current training model we have. However, our results show that there is a lot of potential for this technology since small topologies can be inferred with great accuracy, precision and recall. Now the challenge lies in hugely scaling this technique for hundreds and then hundreds of thousands of neurons.

## References

[1] P. Zhang *et al.*, "High-resolution deep functional imaging of the whole mouse brain by photoacoustic computed tomography in vivo," *Journal of biophotonics*, vol. 11, no. 1, p. e201700024, 2018.

[2] A. P. Alivisatos *et al.*, "Nanotools for neuroscience and brain activity mapping," *ACS Nano*, vol. 3, no. 7, 2013.

[3] I. F. Akyildiz, M. Pierobon, S. Balasubramaniam, and Y. Koucheryavy, "The internet of bio-nano things," *IEEE Communications Magazine*, vol. 53, no. 3, pp. 32–40, 2015.

[4] O. B. Akan, H. Ramezani, T. Khan, N. A. Abbasi, and M. Kuscu, "Fundamentals of molecular information and communication science," *Proceedings of the IEEE*, vol. 105, no. 2, pp. 306–318, 2017.

[5] M. T. Barros, "Ca2+-signaling-based molecular communication systems: Design and future research directions," *Nano Communication Networks*, vol. 11, pp. 103–113, 2017.

[6] A. Coates, A. O. Hero III, R. Nowak, and B. Yu, "Internet tomography," *IEEE Signal processing magazine*, vol. 19, no. 3, pp. 47–65, 2002.

[7] M. T. Barros, "Capacity of the hierarchical multi-layered cortical microcircuit communication channel," in *Proceedings of the 5th ACM International Conference on Nanoscale Computing and Communication*, p. 7, ACM, 2018.

[8] Y. Tsang *et al.*, "Network delay tomography," *IEEE Transactions on Signal Processing*, vol. 51, no. 8, pp. 2125–2136, 2003.

[9] H. Ramezani and O. B. Akan, "Impacts of spike shape variations on synaptic communication," *IEEE Transactions on NanoBioscience*, 2018.

[10] A. L. Hodgkin and A. F. Huxley, "A quantitative description of membrane current and its application to conduction and excitation in nerve," *The Journal of physiology*, vol. 117, no. 4, p. 500, 1952.

[11] W. Rall, "Membrane potential transients and membrane time constant of motoneurons," *Experimental neurology*, vol. 2, no. 5, pp. 503–532, 1960.

[12] H. Markram *et al.*, "Reconstruction and simulation of neocortical microcircuitry," *Cell*, vol. 163, no. 2, pp. 456–492, 2015.